

Carbon Nanotube Transmission between Linear and Rotational Motions

Hanqing Jiang¹, Junqiang Lu², Min-Feng Yu², Yonggang Huang³

Summary

The periodic lattice registry of multi-walled carbon nanotubes (MWCNTs) have been exploited for the possibilities of development of nanodevices. This paper studied the telescoping behaviors of double-walled carbon nanotubes (DWCNTs) by atomic-scale finite element and tight-binding Green function methods. It was found that telescoping a DWCNT (e.g., (6,3)/(12,6)) will induce a rotational motion of the inner CNT that has a chiral angle θ ($0^\circ < \theta < 30^\circ$). This telescoping-induced rotational motion does not exist for armchair and zigzag DWCNTs due to the symmetry of CNTs. The rotational angle is completely determined by the chirality of the inner CNT and can be intuitively explained by screw/nut model. The study of transportation property of (6,3)/(12,6) DWCNT shows a periodic variation of electrical conductance with telescope distance. The period is determined by the lattice constant of graphene (0.246 nm) and chirality of the inner CNT. The unique linear/rotational motions transmission and periodic variation of electrical conductance present fascinating opportunities for the engineering of a new class of nanometrology devices, namely, rotational and distance encoder.

keywords: Double-walled carbon nanotubes; telescoping; rotational motion; electrical conductance

Introduction

The extraordinary strength and unique electrical properties of carbon nanotubes (CNTs) are associated with their highly graphitized lattice structure and cylindrical geometry¹. The possibilities of development of nanodevices utilizing the periodic lattice registry of multi-walled carbon nanotubes (MWCNTs) have been exploited from the experimental^{2,3} and theoretical⁴⁻²⁵ aspects. For example, Cumings and Zettl³ have observed monotonic change of electrical resistance between the ends of a multi-walled carbon nanotube with telescope distance in transmission electron microscopy. By sliding an inner CNT of a MWCNT, Jensen et al² have created a tunable mechanical nanoscale resonator with potential applications in precise mass, force, position, and frequency measurement. Jiang et al⁷ used a tight-binding method to study the electrical conductance of a telescoping double-walled carbon nanotube (DWCNT). The observed periodic oscillation of conductance (~ 0.12

¹Department of Mechanical and Aerospace Engineering, Arizona State University, Tempe, Arizona 85287, USA. hanqing.jiang@asu.edu

²Department of Mechanical Science and Engineering, University of Illinois, Urbana, IL 61801

³Department of Civil and Environmental Engineering and Department of Mechanical Engineering, Northwestern University, Evanston, Illinois 60208, USA

nm) with telescope distance suggests a carbon nanotube electronic displacement encoder with sub-nanometer resolution. Inspired by these recent discoveries of the unique properties of DWCNTs, in this paper we study the rotational motion of the inner CNT induced by its linear (telescope) motion, which can be potentially used as a nano-transmission between the linear and rotational motions.

Methods

Figure 1 illustrates the computational model of a telescope DWCNT. The outer CNT is clamped in order to eliminate rigid-body motion; the inner CNT is pulled out by imposing a uniform displacement at its right end. The second-generation atomistic potential for carbon²⁶ was used to characterize the interactions between covalently bonded carbon atoms; and the Lennard-Jones 12-6 potential²⁷ was used to describe the interlayer interactions between inner- and outer-CNTs. The equilibrium configuration of the telescope DWCNT is then determined by the atomic-scale finite element method (AFEM)^{28,29}.

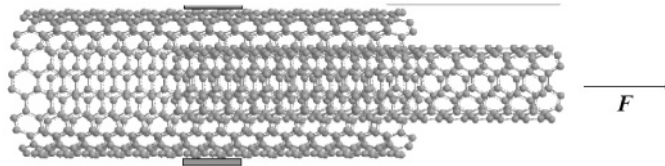


Figure 1: Schematic diagram of a double-walled carbon nanotube (CNT). The outer CNT is fixed, while the inner CNT is pulled out by a uniform displacement at its right end.

The basic idea of AFEM is that static equilibrium corresponds to a state of minimum potential energy. For a system of N atoms, the total potential energy stored in the atomic bonds is

$$E_{tot}(\mathbf{x}) = U_{tot}(\mathbf{x}) - \sum_{i=1}^N \bar{\mathbf{F}}_i \cdot \mathbf{x}_i, \quad (1)$$

where $U_{tot}(\mathbf{x})$ is the atomistic potential energy (e.g., Brenner's potential for carbon and Lennard-Jones potential) that depends on the atom positions $\mathbf{x} = (\mathbf{x}_1, \mathbf{x}_2, \dots, \mathbf{x}_N)^T$, and $\bar{\mathbf{F}}_i$ is the external force (if there is any) exerted on atom i . The state of minimum energy corresponds to

$$\frac{\partial E_{tot}}{\partial \mathbf{x}} = 0. \quad (2)$$

The Taylor expansion of E_{tot} around an initial position $\mathbf{x}^{(0)} = (\mathbf{x}_1^{(0)}, \mathbf{x}_2^{(0)}, \dots, \mathbf{x}_N^{(0)})^T$

of the equilibrium state gives

$$E_{tot}(\mathbf{x}) \approx E_{tot}(\mathbf{x}^{(0)}) + \left. \frac{\partial E_{tot}}{\partial \mathbf{x}} \right|_{\mathbf{x}=\mathbf{x}^{(0)}} \cdot (\mathbf{x} - \mathbf{x}^{(0)}) + \frac{1}{2} (\mathbf{x} - \mathbf{x}^{(0)})^T \cdot \left. \frac{\partial^2 E_{tot}}{\partial \mathbf{x} \partial \mathbf{x}} \right|_{\mathbf{x}=\mathbf{x}^{(0)}} \cdot (\mathbf{x} - \mathbf{x}^{(0)}). \quad (3)$$

The governing equation for the displacement $\mathbf{u} = \mathbf{x} - \mathbf{x}^{(0)}$ is obtained by substituting Eq. (3) into Eq. (2) as follows

$$\mathbf{K}\mathbf{u} = \mathbf{P}, \quad (4)$$

where

$$\mathbf{K} = \left. \frac{\partial^2 E_{tot}}{\partial \mathbf{x} \partial \mathbf{x}} \right|_{\mathbf{x}=\mathbf{x}^{(0)}} = \left. \frac{\partial^2 U_{tot}}{\partial \mathbf{x} \partial \mathbf{x}} \right|_{\mathbf{x}=\mathbf{x}^{(0)}} \quad (5)$$

is the stiffness matrix, and

$$\mathbf{P} = - \left. \frac{\partial E_{tot}}{\partial \mathbf{x}} \right|_{\mathbf{x}=\mathbf{x}^{(0)}} = \bar{\mathbf{F}} - \left. \frac{\partial U_{tot}}{\partial \mathbf{x}} \right|_{\mathbf{x}=\mathbf{x}^{(0)}} \quad (6)$$

is the non-equilibrium force vector, and $\bar{\mathbf{F}} = (\bar{\mathbf{F}}_1, \bar{\mathbf{F}}_2, \dots, \bar{\mathbf{F}}_N)^T$. The stiffness matrix \mathbf{K} and non-equilibrium force vector \mathbf{P} are evaluated in each iteration step. Eq. (6) is solved iteratively until \mathbf{P} reaches zero, which corresponds to the static equilibrium. A similar method was developed by Theodosiou and Saravanos³⁰.

Once the equilibrium configuration is obtained, the transport studies will then be conducted. The DWCNT segment is considered as a conductor, while the single layered portions (outside the DWCNT segment) are modeled as two electrodes. The conductance is determined using a tight-binding³¹ Green's function method within the framework of the Landauer approach^{32,33}. The conductance is given by

$$G = G_0 Tr(\Gamma \Delta_L \Gamma^+ \Delta_R), \quad (7)$$

where G_0 is the quantum conductance ($G_0 = 2e^2/h = 1/12.9 \text{ k}\Omega^{-1}$), Tr is the trace of the matrix, Γ is the Green's function of the conductor, Γ^+ is the conjugate of Γ , and Δ_L and Δ_R are the spectral densities describing the coupling between the conductor and the electrodes.

Results and Discussions

We begin with a (6,3)/(12,6) DWCNT having a commensurate interlayer lattice matching, which has 2700 carbon atoms and is about 12 nm long. Figure 2 shows the snapshots for the (6,3)/(12,6) DWCNT during continuously telescoping. In order to better visualize the motion of the DWCNT, a carbon atom in the outer CNT (fixed) and a string of atoms forming a helix in the inner CNT are marked in yellow. Figure 2a shows the initial equilibrium configuration that corresponds to the telescope distance $d = 0$ nm. The equilibrium configuration for $d = 1$ nm

is shown in Fig. 2b where the marked string of atoms in the inner CNT is moved away from the paper complemented by a counterclockwise rotation. Figures 2c and d further show this rotational motion induced by the linear telescoping motion. We define the rotation angle as the angle deviation from the initial equilibrium positions (Fig. 2a). Figure 3 shows the rotation angle versus the telescope distance d , where an approximately linear relationship is observed. A linear fitting with $36.5^\circ/\text{nm}$ agrees very well with AFEM results. This linear relationship between linear and rotational motions will be discussed further.

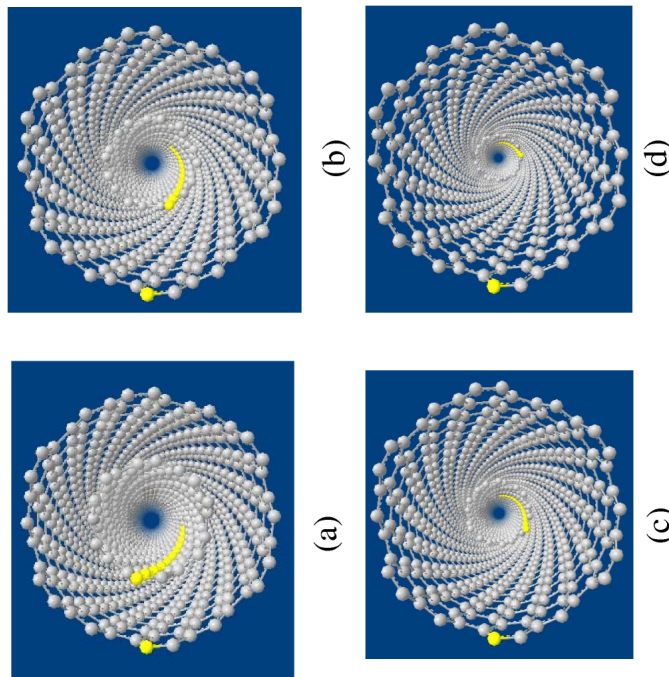


Figure 2: Snapshots when a inner carbon nanotube (CNT) is telescoping from a (6,3)/(12,6) double-walled carbon nanotube for different telescoping distance d : (a) $d = 0$ nm (initial configuration); (b) $d = 1$ nm; (c) $d = 2$ nm; and (d) $d = 3$ nm. In order to better visualize the motion of the inner CNT, a carbon atom (fixed) in the outer CNT and a string of atoms formed a helix in the inner CNT are marked in yellow.

We also study other DWCNTs to test if this telescoping-induced rotational motion is commonplace. Figure 4 shows two DWCNTs (5,5)/(10,10) and (8,0)/(17,0) that have commensurate interlayer lattice matching, as well as a (5,5)/(18,0) DWCNT that has incommensurate interlayer lattice matching. None of these DWCNTs show a relationship between linear (telescoping) and rotational motions.

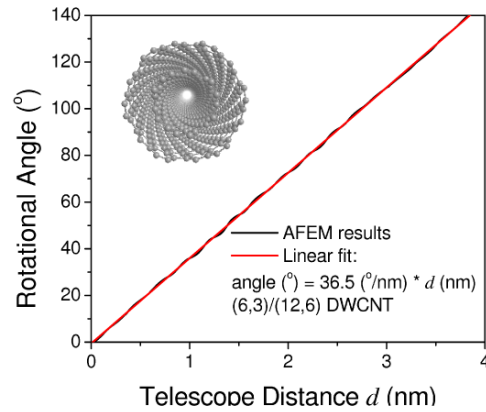


Figure 3: The variation of rotational angle versus telescope distant d for a (6,3)/(12,6) double-walled carbon nanotube.

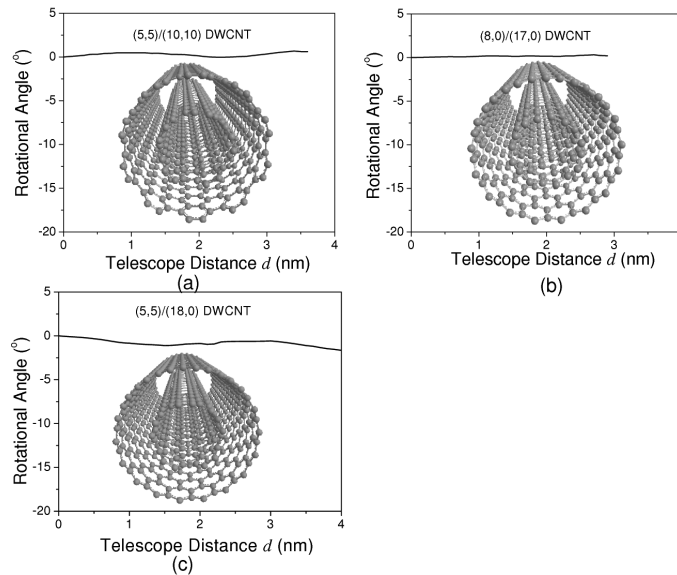


Figure 4: The variation of rotational angle versus telescope distant d for (a) (5,5)/(10,10) double-walled carbon nanotube (DWCNT); (b) (8,0)/(17,0) DWCNT; and (c) (5,5)/(18,0) DWCNT.

The relationship between linear (telescoping) and rotational motions can be intuitively explained by a screw/nut model. Figure 5a shows a screw and nut where a helix is defined. The linear and rotational motion is determined by the nature of this helix, which is similar to Fig. 2, where the (6,3)/(12,6) DWCNT has a helix. One helix is highlighted in yellow in the inner CNT. Other CNTs are describable by a “nail” model. Nails (Fig. 5b) do not have a helix and thus linear motion (e.g., punching) does not lead to rotational motion. A similar situation holds for



Figure 5: Images of (a) screw and nut, and (b) nails, which can explain the unique rotational/linear motion relationship in double-walled carbon nanotubes.

(5,5)/(10,10), (8,0)/(17,0) and (5,5)/(18,0) DWCNTs (Fig. 4).

The quantitative interpretation is given by the chiral angle of CNTs. A CNT can be considered as a rolled graphene sheet (Fig. 6). Following the standard notation for CNTs, the chiral vector \mathbf{C}_h , whose length equals the circumference of the CNT, can always be expressed in terms of the unit vectors (\mathbf{a}_1 and \mathbf{a}_2) in the planar hexagonal lattice as

$$\mathbf{C}_h = n\mathbf{a}_1 + m\mathbf{a}_2, \quad (8)$$

where a pair of integers (n, m) is called the chirality of the CNT. When the graphene is rolled up to form the cylindrical nanotube, the ends of the chiral vector (e.g., points O and A in Fig. 6) meet each other. The chiral vector thus forms the circumference of the CNT's circular cross-section, and different values of n and m lead to different CNTs structures, namely armchair ($n = m$), zigzag ($m = 0$), and chiral CNTs ($n > m > 0$). Perpendicular to the chiral vector \mathbf{C}_h , \mathbf{T} is the translational vector, which is the axial direction of the CNTs. In other words, rectangle $OAB'B$ in Fig. 6 forms a (6,3) chiral CNT.

Noting that for graphene, $|\mathbf{a}_1| = |\mathbf{a}_2| = a$ (though it is slightly different for CNTs with radius effect³⁴), the circumference of the CNT is

$$|\mathbf{C}_h| = \sqrt{\mathbf{C}_h \cdot \mathbf{C}_h} = \sqrt{n^2 + m^2 + nma}, \quad (9)$$

and the CNT radius is

$$r = \frac{|\mathbf{C}_h|}{2\pi}. \quad (10)$$

The chiral angle θ , which is the angle between $|\mathbf{C}_h|$ and \mathbf{a}_1 , is similarly obtained in terms of the chirality (n, m) as

$$\theta = \cos^{-1} \frac{\mathbf{C}_h \cdot \mathbf{a}_1}{|\mathbf{C}_h|a} = \cos^{-1} \frac{2n + m}{2\sqrt{n^2 + m^2 + nm}}. \quad (11)$$

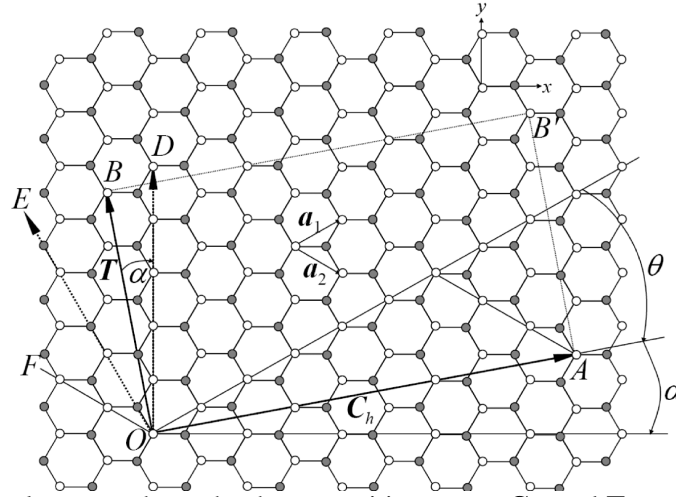


Figure 6: A planar graphene that has quantities \mathbf{a}_1 , \mathbf{a}_2 , \mathbf{C}_h , and \mathbf{T} to characterize a carbon nanotube.

The chiral angle is 30° for armchair CNTs, and 0° for zigzag CNTs, while it is intermediate between 0° and 30° for chiral CNTs. The angle α is defined between the translational vector \mathbf{T} and the vertical axis (y -axis) and is associated with the chiral angle θ as

$$\alpha = \frac{\pi}{6} - \theta. \quad (12)$$

The angle α is 0° for armchair CNTs, 30° for zigzag CNTs and between 0° and 30° for chiral CNTs.

It is well known that there are two equivalent sublattices for graphene (and hence the CNTs), marked by filled and open circles in Fig. 6. For armchair CNTs ($\alpha = 0^\circ$), all atoms in the translational vector \mathbf{T} (along the \overrightarrow{OD} direction) belong to the same sublattice (marked by open circles). For zigzag CNTs ($\alpha = 30^\circ$), atoms along the translational vector (\overrightarrow{OE} direction) form a filled-open mixed, periodic pattern, and the atoms from the same sublattice (e.g., atoms marked by open circles along \overrightarrow{OD} and \overrightarrow{OF} directions) are symmetric about the translational vector (along \overrightarrow{OE} direction). However, the atoms from the same sublattice (e.g., open circles along \overrightarrow{OD} and \overrightarrow{OF} directions) in chiral CNTs do not form a symmetric pattern about the translational vector (along \overrightarrow{OB} direction). The angle $\varphi = \min(\alpha, \theta)$ forms the helix for chiral CNTs.

When the CNT is subject to linear motion along its axial direction (translational vector \mathbf{T}), the symmetry of atoms forming from the same sublattice about the axial direction prevents the CNT from rotational motion, which holds for armchair and zigzag CNTs. However, for chiral CNTs, the asymmetry of atoms forming from

the same sublattice about the axial direction leads to rotational motion due to linear motion, i.e., the atoms tend to rotate clockwise with angle φ , such that the angle that the inner CNT rotates per linear motion is

$$\beta = \frac{\tan(\varphi)}{r} = \frac{\tan\left[\min\left(\cos^{-1}\frac{2n+m}{2\sqrt{n^2+m^2+nm}}, \frac{\pi}{6} - \cos^{-1}\frac{2n+m}{2\sqrt{n^2+m^2+nm}}\right)\right]}{\sqrt{n^2+m^2+nm}}, \quad (13)$$

where (n, m) and r are the chirality and radius (Eq. 10) of the inner CNT.

Based on this analysis, the angle that the (6,3) inner CNT rotates in (6,3)/(12,6) DWCNT is $35.5^\circ/\text{nm}$, which agrees very well with the linear fitting given in Fig. 3. Here $a = 0.246$ nm has been used. The slight difference between the present analysis and linear fitting may be because of the slight difference between bond length for planar graphene and cylindrical CNT as discussed by Jiang et al³⁴. In order to further verify the present analysis, we also study a (7,4)/(12,9) DWCNT that has different chiral angles for inner and outer CNTs. As shown in Fig. 7, the rotational angle per telescope distance is $24.5^\circ/\text{nm}$, which agrees very well with the present analysis based on Eq. (13) for $\beta = 23.9^\circ/\text{nm}$.

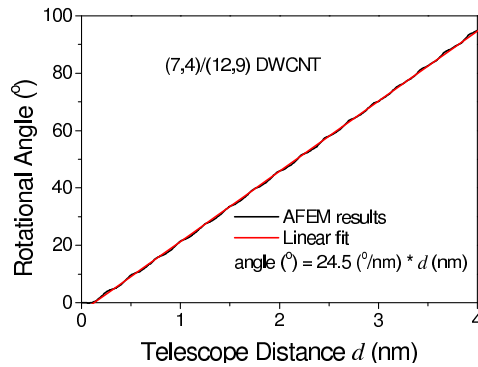


Figure 7: The variation of rotational angle versus telescope distant d for a (7,4)/(12,9) double-walled carbon nanotube.

The novel transmission between linear and rotational motions can be potentially used in a rotational or distance encoder. In order to accurately measure the telescope distance, and hence the induced rotational angle, we also calculate the electrical conductance change with telescope distance, similar to Jiang et al⁷.

Figure 8 shows the conductance variation in telescoping a (6,3)/(12,6) DWCNT. The conductance varies periodically as the inner CNT is pulled out continuously. The variation has a stable period of 0.24 nm ($= a \cos \varphi$). Since $0 \leq \varphi \leq 15^\circ$ for all kinds of inner CNTs, the difference between the period and the lattice constant of graphene ($a = 0.246$ nm) will be less than 4%. This transport behavior and the lattice constant periodicity suggest such a telescope DWCNT device can function as a

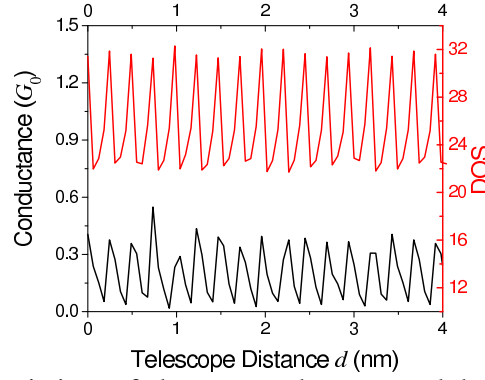


Figure 8: Periodic variations of electron conductance and density of states (DOS) with telescope distance for a (6,3)/(12,6) double-walled carbon nanotube. $G_0 = 2e^2/h = 1/12.9 \text{ k}\Omega^{-1}$.

sub-nanometer resolution displacement encoder and provide absolute displacement measurement traceable to a physical constant.

The correlation between the variations of conductance and density of states (DOS) is obvious. The maxima in conductance are found to correspond to the maxima in the DOS, contrary to the studied by Jiang et al⁷. In other words, the (6,3)/(12,6) DWCNT does not exhibit an antiresonance in transmission. The mechanism of absence of antiresonance in transmission can be explained by the antiresonance condition

$$(k_1 + k_2)L + \theta_0 = 2n\pi, \quad (14)$$

where k_1 and k_2 are wave vectors for inner and outer CNTs, L is the length of the double-walled segment, θ_0 is the initial phase difference in wave functions, and n is an integer. Under zero external bias, we can reasonably assume that the values of k_1 and k_2 for the energy levels at the hybrid region remain very close to Fermi energy k_F at the Fermi surface of either a (6, 3) or a (12, 6) CNT which is zero³⁵. Thus, the antiresonance does not occur for (6,3)/(12,6) DWCNTs.

Conclusion Remarks

The telescoping behaviors of DWCNTs have been studied by AFEM and a tight-binding method. It was found that telescoping a DWCNT (e.g., (6,3)/(12,6) where the inner CNT has a chiral angle θ ($0^\circ < \theta < 30^\circ$)) will induce a rotational motion of the inner CNT. The rotational angle is determined by the chirality of the inner CNT to be $\tan \varphi/r$, where $\varphi = \min(\theta, \frac{\pi}{6} - \theta)$, and r is the radius of the inner CNT. This telescoping-induced rotational motion does not exist for armchair and zigzag DWCNTs due to the symmetry of these CNTs. The linear/rotational motion transmission can be intuitively explained by a screw/nut model. The study of transportation properties of (6,3)/(12,6) DWCNT shows a periodic variation of electrical

conductance with telescope distance. The variation has a stable period (0.24 nm), which is close to the lattice constant of graphene. The unique linear/rotational motion transmission and periodic variation of electrical conductance present fascinating opportunities for the engineering of a new class of nanometrology devices, namely rotational and distance encoders.

Acknowledgement

HJ acknowledges the financial support from the Fulton School of Engineering at ASU. MFY and HY acknowledge the support from the NSF CCF-0508416.

References

1. J. Bernholc, D. Brenner, M. B. Nardelli et al., 2002. Mechanical and electrical properties of nanotubes. *Ann. Rev. Mater. Res.* **32**, 347-375.
2. K. Jensen, C. Girit, W. Mickelson et al., 2006. Tunable nanoresonators constructed from telescoping nanotubes. *Phys. Rev. Lett.* **96** (21), 4.
3. J. Cumings and A. Zettl, 2004. Localization and nonlinear resistance in telescopically extended nanotubes. *Phys. Rev. Lett.* **93** (8), 4.
4. M. Upmanyu and J. R. Barber, 2005. Interrupted tubules in filamentous crystals: Elastic analysis. *Phys. Rev. B* **72** (20), 6.
5. P. Liu, Y. W. Zhang, and C. Lu, 2006. Analysis of the oscillatory behavior of double-walled carbon nanotube-based oscillators. *Carbon* **44** (1), 27-36.
6. W. L. Guo and H. J. Gao, 2005. Optimized bearing and interlayer friction in multiwalled carbon nanotubes. *CMES-Comp. Model. Eng. Sci.* **7** (1), 19-34.
7. H. Jiang, M. F. Yu, J. Q. Lu et al., 2007. Carbon nanotube electronic displacement encoder with sub-nanometer resolution. *J. Comput. Theor. Nanosci.* **4** (3), 574-577.
8. A. Hansson and S. Stafstrom, 2003. Intershell conductance in multiwall carbon nanotubes. *Phys. Rev. B* **67** (7), 6.
9. S. Uryu, 2004. Electronic states and quantum transport in double-wall carbon nanotubes. *Phys. Rev. B* **69** (7), 10.
10. I. M. Grace, S. W. Bailey, and C. J. Lambert, 2004. Electron transport in carbon nanotube shuttles and telescopes. *Phys. Rev. B* **70** (15), 4.
11. Y. K. Kwon and D. Tomanek, 1998. Electronic and structural properties of multiwall carbon nanotubes. *Phys. Rev. B* **58** (24), R16001-R16004.
12. Y. Miyamoto, S. Saito, and D. Tomanek, 2002. Electronic interwall interactions and charge redistribution in multiwall nanotubes. *Phys. Rev. B* **65** (4), 4.

13. D. H. Kim, H. S. Sim, and K. J. Chang, 2001. Electronic and transport properties of single-wall carbon nanotubes encapsulating fullerene-based structures. *Phys. Rev. B* **64**(11), 7.
14. D. H. Kim and K. J. Chang, 2002. Electron transport in telescoping carbon nanotubes. *Phys. Rev. B* **66**(15), 5.
15. X. F. Li, K. Q. Chen, L. L. Wang et al., 2007. Effect of intertube interaction on the transport properties of a carbon double-nanotube device. *J. Appl. Phys.* **101**(6), 4.
16. A. Subramanian, L. X. Dong, J. Tharian et al., 2007. Batch fabrication of carbon nanotube bearings. *Nanotechnology* **18**(7), 9.
17. S. Uryu and T. Ando, 2006. Impurity induced inter-tube conductance in double-wall carbon nanotubes. *Phys. Status Solidi B-Basic Solid State Phys.* **243**(13), 3281-3284.
18. M. A. Tunney and N. R. Cooper, 2006. Effects of disorder and momentum relaxation on the intertube transport of incommensurate carbon nanotube ropes and multiwall nanotubes. *Phys. Rev. B* **74**(7), 16.
19. S. Uryu and T. Ando, 2005. Electronic intertube transfer in double-wall carbon nanotubes. *Phys. Rev. B* **72**(24), 10.
20. Q. M. Yan, J. Wu, G. Zhou et al., 2005. Ab initio study of transport properties of multiwalled carbon nanotubes. *Phys. Rev. B* **72**(15), 5.
21. J. W. Kang, K. O. Song, O. K. Kwon et al., 2005. Carbon nanotube oscillator operated by thermal expansion of encapsulated gases. *Nanotechnology* **16**(11), 2670-2676.
22. Z. C. Tu and X. Hu, 2005. Molecular motor constructed from a double-walled carbon nanotube driven by axially varying voltage. *Phys. Rev. B* **72**(3), 4.
23. Z. C. Tu and Z. C. Ou-Yang, 2004. A molecular motor constructed from a double-walled carbon nanotube driven by temperature variation. *J. Phys.-Condes. Matter* **16**(8), 1287-1292.
24. J. Han, A. Globus, R. Jaffe et al., 1997. Molecular dynamics simulations of carbon nanotube-based gears. *Nanotechnology* **8**(3), 95-102.
25. D. Srivastava, 1997. A phenomenological model of the rotation dynamics of carbon nanotube gears with laser electric fields. *Nanotechnology* **8**(4), 186-192.

26. D. W. Brenner, O. A. Shenderova, J. A. Harrison et al., 2002. A second-generation reactive empirical bond order (REBO) potential energy expression for hydrocarbons. *J. Phys.-Condes. Matter* **14** (4), 783-802.
27. L. A. Girifalco, M. Hodak, and R. S. Lee, 2000. Carbon nanotubes, buckyballs, ropes, and a universal graphitic potential. *Phys. Rev. B* **62** (19), 13104-13110.
28. B. Liu, H. Jiang, Y. Huang et al., 2005. Atomic-scale finite element method in multiscale computation with applications to carbon nanotubes. *Phys. Rev. B* **72** (3), 8.
29. B. Liu, Y. Huang, H. Jiang et al., 2004. The atomic-scale finite element method. *Comput. Meth. Appl. Mech. Eng.* **193** (17-20), 1849-1864.
30. T. C. Theodosiou and D. A. Saravanos, 2007. Molecular mechanics based finite element for carbon nanotube modeling. *CMES-Comp. Model. Eng. Sci.* **19** (2), 121-134.
31. P. Lambin, V. Meunier, and A. Rubio, 2000. Electronic structure of polychiral carbon nanotubes. *Phys. Rev. B* **62** (8), 5129-5135.
32. S. Datta, *Electronic Transport in Mesoscopic Systems*. (Cambridge University Press, Cambridge, 1995).
33. J. Q. Lu, J. Wu, W. H. Duan et al., 2003. Metal-to-semiconductor transition in squashed armchair carbon nanotubes. *Phys. Rev. Lett.* **90** (15), 4.
34. H. Jiang, P. Zhang, B. Liu et al., 2003. The effect of nanotube radius on the constitutive model for carbon nanotubes. *Comput. Mater. Sci.* **28** (3-4), 429-442.
35. R. Saito, G. Dresselhaus, and M. S. Dresselhaus, *Physical Properties of Carbon Nanotubes*. (Imperial College Press, London, 1998).